Identification of Conformational Substates Involved in Nitric Oxide Binding to Ferric and Ferrous Myoglobin through Difference Fourier Transform Infrared Spectroscopy (FTIR)†

Lisa M. Miller,§,‖ Ana J. Pedraza,‡ and Mark R. Chance*,‡

Department of Physiology and Biophysics, Albert Einstein College of Medicine of Yeshiva University, Bronx, New York 10461, and Division of Energy and Environment, Lawrence Berkeley National Laboratory, MS 2-300, 1 Cyclotron Road, Berkeley, California 94720

Received November 4, 1996; Revised Manuscript Received July 21, 1997⊗

ABSTRACT: Hemeproteins play an important role in the signaling processes mediated by nitric oxide (NO). For example, the production of NO by nitric oxide synthase, the activation of guanylate cyclase by binding NO, and the scavenging of NO by hemoglobin, myoglobin, and cytochrome *c* oxidase all occur through unique mechanisms of interaction between NO and hemeproteins. Unlike carbon monoxide (CO) and oxygen (O_2), which have been studied extensively, the reactions of NO with ferric and ferrous hemeproteins are not as well characterized. In this work, NO binding to myoglobin is studied using cryogenic optical spectroscopy and Fourier transform infrared spectroscopy (FTIR) in order to characterize the ligand-bound and photoproduct states involved in the interaction of NO with the heme iron and the distal pocket of the protein. For ferrous nitrosyl myoglobin ($Mb^{II}NO$), optical spectroscopy is used to show that the ligand-bound state can be converted to >95% stable photoproduct below 10 K. The Soret peak of the photoproduct is red-shifted by 4 nm relative to deoxy-myoglobin (Mb), similar to previous results for carbonmonoxy- (MbCO) and oxy-myoglobin (MbO_2) (Miller et al., 1996). $Mb^{II}NO$ completely rebinds by 35 K, indicating that the rebinding barrier for NO is lower than MbCO, consistent with room temperature picosecond kinetic measurements. For ferric nitrosyl myoglobin ($Mb^{III}NO$), we find that the photoproduct yield at cryogenic temperatures is less than unity and dependent on the distal pocket residue. Native $Mb^{III}NO$ has a lower photoproduct yield than the mutant, Mb^{III}(H64L)NO, where the distal histidine is replaced by leucine. The rebinding rates for the native and mutant species are similar to each other and to $Mb^{II}NO$. By using FTIR difference spectroscopy (photolyzed/unphotolyzed) of isotopically labeled ferrous nitrosyl myoglobin ($Mb^{II}NO$), the NO stretching frequencies in both the ligand-bound states and photoproduct states are determined. Two ligand-bound conformational states (1607 and 1613 cm^{-1}) and two photoproduct conformational states (1852 and 1857 cm^{-1}) are observed for $Mb^{II}NO$. This is the first direct observation of photolyzed NO in the distal pocket of myoglobin. The ligand-bound frequencies are consistent with a bent $Mb^{II}NO$ moiety, where the unpaired π^*(NO) electron remains localized on NO, causing ν(N−O) to be ∼300 cm^{-1} lower than $Mb^{III}NO$. Similar to MbO_2, we suggest that N_ϵ of the distal histidine is protonated, forming a hydrogen bond to the NO ligand. For native $Mb^{III}NO$, a single ligand-bound conformational state with respect to ν(N−O) is observed at 1927 cm^{-1}. This frequency *decreases* to 1904 cm^{-1} for the mutant, Mb^{III}(H64L)NO, contrary to the *increase* of the carbon monoxide (CO) stretching frequency in the isoelectronic Mb^{II}(H64L)CO mutant versus native MbCO. For linear $Mb^{III}NO$, we suggest that backbonding from the unpaired π^*(NO) electron to iron results in an increased positive charge on the NO ligand, $Fe^{(\delta-)}-NO^{(\delta+)}$. This can be facilitated by tautomerism of the distal histidine, leaving N_ϵ of the imidazole ring unprotonated and able to accept positive charge from the $Fe^{(\delta-)}-NO^{(\delta+)}$ moiety, resulting in a higher bond order (and a 23 cm^{-1} shift to higher frequency) for native $Mb^{III}NO$ versus Mb^{III}(H64L)NO, where this interaction is absent. These different interactions between the distal histidine and the ferrous versus ferric species illustrate potential ways the protein can stabilize the bound ligand and demonstrate the versatile nature by which NO can bind to hemeproteins.

Nitric oxide (NO) is produced by the heme-containing nitric oxide synthase, and plays a role in physiological processes such as neurotransmission, vasodilatation, lymphocyte proliferation, and platelet activity (Jia et al., 1996; Moncada & Higgs, 1993; Nathan, 1992; Stamler et al., 1992). Hemeproteins have long been known to react with nitric oxide, but the widespread and diverse nature of these interactions has only recently become apparent. NO is capable of binding to a variety of hemeprotein environments, which can differ in iron oxidation state, iron spin state, iron coordination number, proximal ligand, and distal pocket environment. For example, the heme iron in the resting state of NO synthase (NOS) is ferric and five-coordinate with a cysteine thiolate as the proximal ligand (Stuehr & Ikeda-

† This research was supported by the NIH Grant HL-45892 (M.R.C.). L.M.M. was supported by a University of California President's Postdoctoral Fellowship.

* Author to whom correspondence should be addressed. Phone: (718) 430-4136. E-mail: mrc@aecom.yu.edu.

‡ Albert Einstein College of Medicine.

§ Lawrence Berkeley National Laboratory.

‖ Present address: Center for Synchrotron Biosciences, Albert Einstein College of Medicine and The National Synchrotron Light Source, Brookhaven National Laboratory, Upton, NY 11973.

⊗ Abstract published in *Advance ACS Abstracts,* September 15, 1997.

S0006-2960(96)02744-4 CCC: $14.00

Saito, 1992). When L-arginine binds to the distal pocket of NOS, it sterically inhibits the binding of ligands to the heme iron. It also induces a less negative reduction potential for the heme iron, leading to reduction of the heme and O_2 binding (Matsuoka et al., 1994). In guanylate cyclase, an enzyme which catalyzes the conversion of GTP to cGMP, NO binds to a ferrous heme iron, stimulating cleavage of the iron-proximal histidine bond in trans (Stone & Marletta, 1994). NO also binds to myoglobin, hemoglobin, cytochrome *c* oxidase, and cytochrome P-450, all of which can affect NO transport from NOS to target sites, such as guanylate cyclase (Brudwig et al., 1980; Ignarro et al., 1993; Jia et al., 1996).

The binding of nitric oxide to ferrous myoglobin has been studied extensively at room temperature in the picosecond time regime. A recent review by Olson and Phillips (1996) illustrates that the barrier to NO binding is governed exclusively by the rate of ligand-entry into the distal pocket, since NO is extremely reactive with the heme iron once it is inside the protein. Thus, steric and electronic interactions between NO and the distal pocket residues are crucial for determining the rebinding barrier. One particularly important residue is the distal histidine, which has been shown to form a hydrogen bond to O_2 (Phillips, 1980; Phillips & Schoenborn, 1981) and probably NO (Ikeda-Saito et al., 1991; Kappl & Hutterman, 1989; Lee et al., 1994), stabilizing the bound ligand. Upon photolysis, it is thought that the distal histidine pushes the ligand to the back of the distal pocket, inhibiting rebinding. Mutation of the distal histidine by smaller and/or apolar residues removes this barrier, resulting in rapid NO recombination (Quillin et al., 1995).

Fourier transform infrared spectroscopy is an excellent method for probing ligand binding and dynamics in hemeproteins. The infrared stretching frequency of NO is sensitive to factors such as the oxidation state of the heme, the orientation of the NO ligand with respect to the heme, and the amino acid composition of the distal pocket. Unfortunately, when NO is bound to ferrous hemes, ν(N−O) falls in the region of the Amide I protein band (∼1600 cm^{-1}). Because the intensity of ν(N−O) is very weak with respect to the Amide I band, difference FTIR spectroscopy is necessary to determine ν(N−O). Recently, Caughey and co-workers investigated NO-binding to myoglobin and cytochrome *c* oxidase using $^{14}NO/^{15}NO$ FTIR difference spectroscopy (Zhao et al., 1994). The authors identified a single ν(N−O) for the ligand-bound state of ferrous myoglobin at 1612 cm^{-1}. However, this difference technique can be extremely difficult because sample concentrations and pathlengths must be matched in order to obtain a good difference spectrum.

We have chosen an alternative approach for probing NO binding in hemeproteins − FTIR photolyzed/unphotolyzed difference spectroscopy. In many hemeproteins, the bond between the heme iron and diatomic ligands such as CO, O_2, and NO can be broken with light. If the photolysis is carried out at cryogenic temperatures, the photoproduct intermediates can be trapped and characterized (Ansari et al., 1987; Austin et al., 1975; Chance, 1993). Previously, our group has utilized this difference technique for identifying the ligand-bound dioxygen stretching frequency in MbO_2 and $CoMbO_2$, the ligand-bound and photolyzed CO stretching frequency in MbCO, and photolysis-sensitive heme and proximal histidine modes in MbO_2 (Chance et al., 1987; Miller & Chance, 1994, 1995). In this study, we take advantage of the photolabile Fe−NO bond in MbNO and generate photolyzed/unphotolyzed FTIR difference spectra at cryogenic temperatures. The advantages of this method over other difference techniques include: (1) a single sample is used to obtain a difference spectrum, so sample-matching is not necessary, (2) both the ligand-bound states and photoproduct states can be obtained in a single experiment, and (3) information about rebinding rates *from* the photoproduct states *to* the ligand-bound states is also obtained.

EXPERIMENTAL PROCEDURES

Preparation of Myoglobin Samples

Horse skeletal muscle myoglobin (95−100%, Sigma) was dissolved in 150 mM potassium phosphate buffer at pH 6.6 (75:25 glycerol:water solvent by volume) and stirred on ice for 10 min. Samples were centrifuged for 20 min at 15000 rpm at 10 °C and then transferred to a nitrogen-purged glovebox, where the samples were thoroughly degassed. For ferrous samples, a two-fold excess of sodium dithionite (Aldrich) was added to reduce the iron to the Fe^{II} state. After stirring 10 min, nitric oxide (^{14}NO: 99 atom %, MG Industries; ^{15}NO: 97 atom %, Isotec) was bubbled through a degassed solution of 0.1 N NaOH, then through a degassed solution of buffer, and finally over the sample for 10 minutes. Optical spectra indicated the samples to be greater than 95% nitrosyl myoglobin, as indicated by a Soret peak at 422 nm (Figure 1) and Q bands at 544 and 574 nm for $Mb^{II}NO$ and by a Soret peak at 420 nm (Figure 2) and Q bands at 536 and 564 nm for $Mb^{III}NO$. For the mutant Mb(H64L)NO, Mb(H64L)CO was first prepared as described by Springer and Sligar (1987). The Mb(H64L)CO sample was concentrated to 3 mM. The CO was removed and the sample oxidized to Mb^{III}(H64L) by photolysis under N_2 gas for 14 h at 10 °C. NO gas was then introduced for 10 min to produce Mb^{III}(H64L)NO.

FTIR Methods for Determining MbNO Substates

MbNO samples (2−5 mM) were placed between two CaF_2 windows using a 0.025 mm teflon spacer and mounted into a N_2-purged, low-temperature cryostat (Janis ST-4B). Samples were cooled to 220 K. Then the cryostat was evacuated to <5 mTorr, and the samples were cooled to 7 K. An optical spectrum of the unphotolyzed MbNO sample was taken inside the cryostat (Figure 1) using a Hewlett Packard HP8452 diode array spectrometer. The sample was subsequently photolyzed for 5 min with a white light source (CUDA Products, Inc., model I-150). The photolysis source was turned off and an optical spectrum of the photolyzed sample was taken (Figure 1). The cryostat was then transferred to a Mattson Galaxy 5000 FTIR spectrometer.

The FTIR spectrometer was thoroughly purged with nitrogen gas (blow-off from a liquid nitrogen dewar) prior to collecting data, to remove all water vapor and CO_2 from the infrared beam path. The spectrometer was considered sufficiently purged when the ratio of two "air" spectra yielded a noise spectrum with a peak-to-peak ratio of $\leq 10^{-4}$ OD units in the infrared region between 1500−1900 cm^{-1}. Spectral interferograms (128 scans) were collected from 900 to 4000 cm^{-1} with 2 cm^{-1} resolution and Fourier transformed

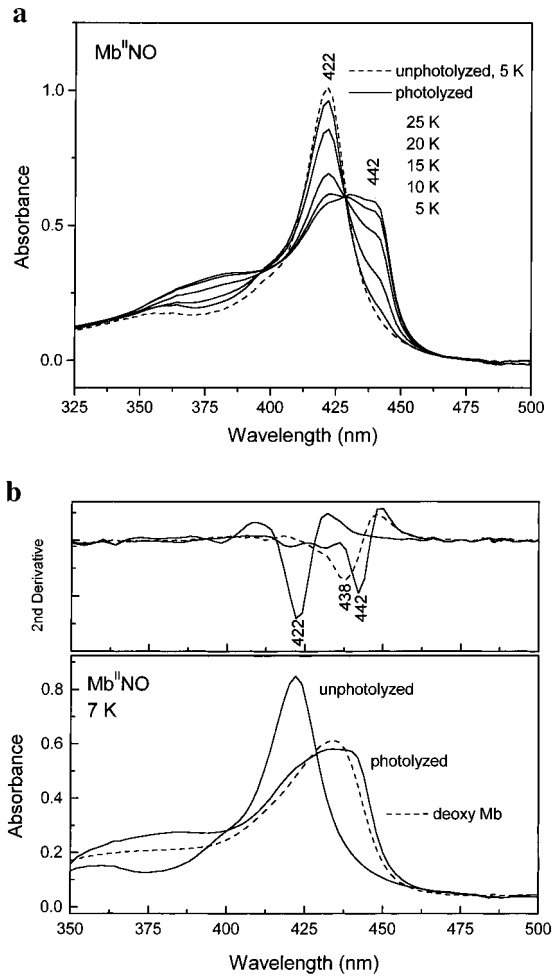

FIGURE 1: (a) Optical spectra of photolyzed (—) and unphotolyzed (- - -) Mb^{II}NO at the specified temperature. (b) Optical spectra (bottom) and second derivatives (top) of photolyzed and unphotolyzed Mb^{II}NO at 7 K and deoxy Mb at room temperature. Samples (2−5 mM in 75:25 glycerol:buffer solution by volume) were placed between two CaF_2 windows with a pathlength of 0.025 mm. Photolysis was performed at 7 K with a high-intensity white light source for 10 min.

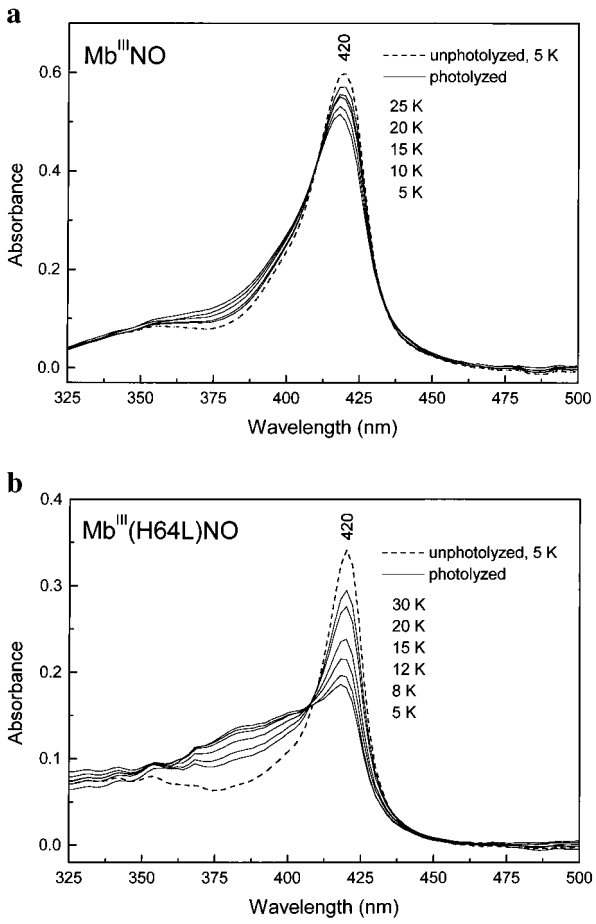

FIGURE 2: (a) Optical spectra of photolyzed (—) and unphotolyzed (- - -) Mb^{III}NO at the specified temperature. (b) Optical spectra of photolyzed (—) and unphotolyzed (- - -) Mb^{III}(H64L)NO at the specified temperature. Sample details and the photolysis protocol are described in Figure 1.

using FIRST software (Mattson, Inc.). After collecting the FTIR spectrum of the photolyzed sample at 7 K, the liquid helium flow was reduced and spectra were collected at 10, 15, 20, 25, and 30 K as the sample was warmed. Difference spectra were generated by dividing the photolyzed MbNO spectrum at 7 K by the partially-rebound spectra at 10, 15, 20, 25, and 30 K, respectively, and converting from transmittance to absorbance units. Using Spectra Calc software (Galactic Industries), we fitted the spectra to a cubic polynomial base line in the region from 1550 to 1650 cm^{-1} and 1800 to 2000 cm^{-1}.

RESULTS

Photoproduct Yields of Mb^{II}NO and Mb^{III}NO

In order for photolyzed/unphotolyzed difference FTIR spectroscopy to be useful in studying ν(N−O), the NO ligand must be photolyzable, i.e. the amount of stable photoproduct produced at cryogenic temperatures (*the photoproduct yield*) must be large enough to obtain a reasonable difference spectrum. This quantity is ∼20% or greater for ligands such as CO and NO, which have reasonably strong oscillator strengths. The optical spectra of photolyzed and unphotolyzed Mb^{II}NO at 7 K can be seen in Figure 1. Absorption peaks for ligand-bound (unphotolyzed) Mb^{II}NO fall at 422, 544, and 574 nm. Upon photolysis at 7 K, the absorption spectrum is converted to an absorption spectrum similar to that of deoxy Mb, suggesting a photoproduct yield of ∼1.0 for Mb^{II}NO. However, second derivative analysis shows that Mb*NO is not identical to deoxy Mb; the Mb*NO spectrum is broader and shifted to higher energy as compared to deoxy Mb (Figure 1b). Upon warming, Mb*NO rebinds by 35 K whereas Mb*CO does not rebind completely until ∼80 K, indicating that the rebinding barrier for NO is lower than CO.

For Mb^{III}NO and Mb^{III}(H64L)NO, the optical spectra for the ligand-bound and photoproduct states can be seen in Figure 2. Upon photolysis, the Soret decreases in intensity and a broad absorption band arises at ∼390 nm. For both the native and the mutant samples, the photoproduct yield appears to be less than unity, where the degree of photolysis in the native Mb^{III}NO sample is significantly less than for the mutant species. Optical studies on ferric, five-coordinate, mutant myoglobins indicate Soret absorption maxima near 393 nm (Morikis et al., 1989; Quillin et al., 1993), consistent with these results. Upon warming, both the native and mutant Mb^{III}NO completely rebind by 35 K, similar to the ferrous species.

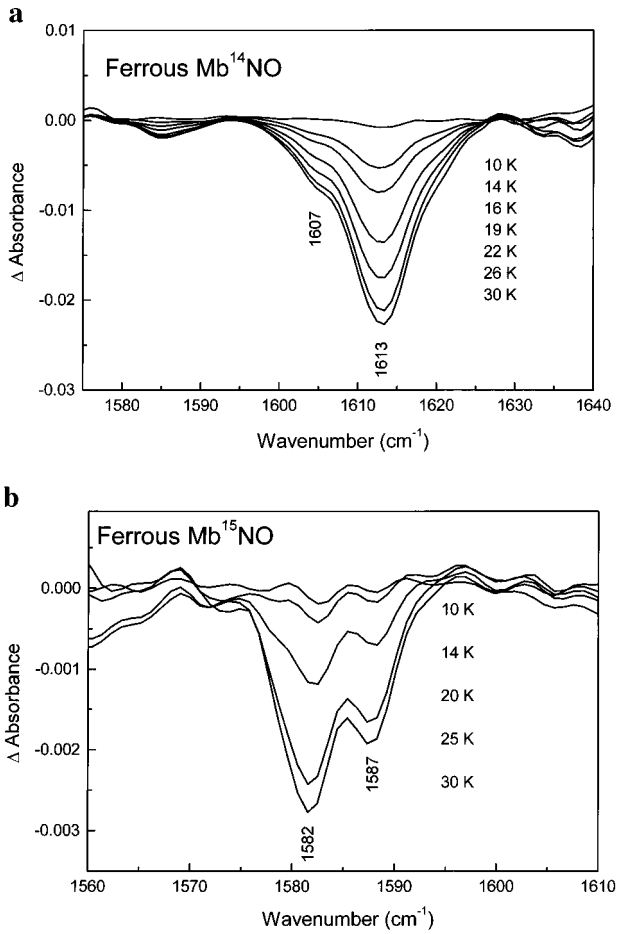

FIGURE 3: FTIR (photolyzed/unphotolyzed) difference spectra of (a) ferrous $Mb^{14}NO$ and (b) ferrous $Mb^{15}NO$, demonstrating the ligand-bound conformational substates of $Mb^{II}NO$. Photolysis was performed at 7 K with a high-intensity white light source for 10 min. Difference spectra were generated by dividing the photolyzed MbNO spectrum at 7 K by the partially-rebound spectra at each indicated temperature.

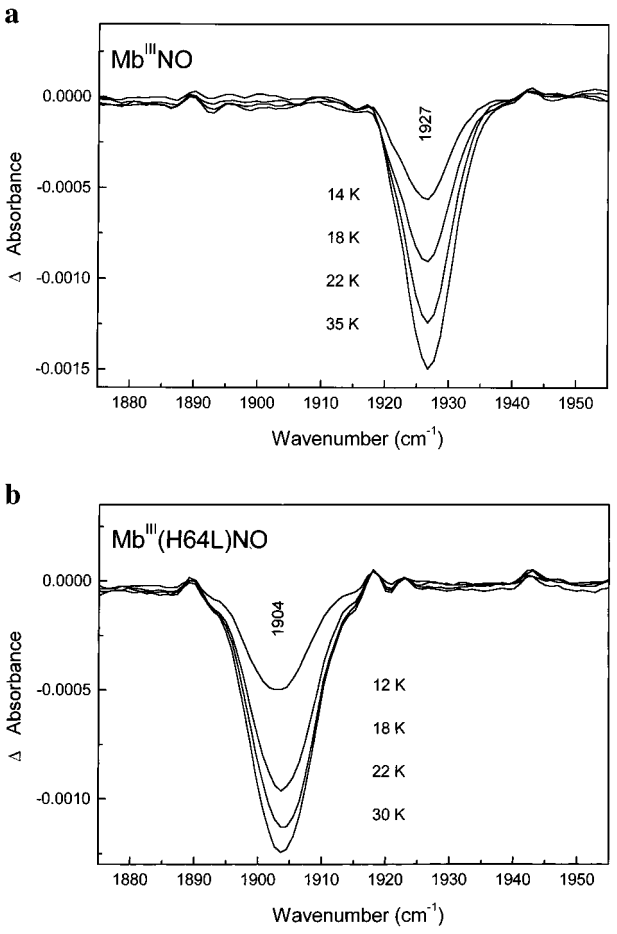

FIGURE 4: FTIR (photolyzed/unphotolyzed) difference spectra of (a) $Mb^{III}NO$ and (b) $Mb^{III}(H64L)NO$ demonstrating the ligand-bound conformational substates. Sample details, the photolysis protocol, and the method for generating difference spectra are described in Figure 3.

Ligand-Bound States of MbNO

Figure 3 shows the photolyzed/unphotolyzed FTIR difference spectra of $Mb^{II}NO$. The primary ligand-bound state falls at 1613 cm^{-1} in $Mb^{14}NO$ (Figure 3a) and shifts to 1587 cm^{-1} in $Mb^{15}NO$ (Figure 3b). A less-populated ligand-bound state is found at 1607 cm^{-1} in $Mb^{14}NO$ and shifts to 1582 cm^{-1} in $Mb^{15}NO$. The band at 1582 cm^{-1} in the $Mb^{15}NO$ spectrum has a greater intensity than predicted from the $Mb^{14}NO$ spectrum because it overlaps with a photolysis-sensitive Amide II band (Figure 3a). The isotopic shifts of both ligand-bound states are slightly less than those predicted by reduced mass calculation for $^{14}NO \rightarrow {}^{15}NO$, which are $\sim$29 cm^{-1}. This small difference can be attributed to the ferrous iron bonded to the NO ligand, which would decrease the difference in reduced masses between ^{14}NO and ^{15}NO, thus decreasing the calculated shift. By qualitatively examining the relative absorption intensities of each substate as a function of temperature, Berendzen and Braunstein (1990) have shown that relative rebinding rates for the ligand-bound states of myoglobin can be determined. Thus, since Figure 3 shows that both ligand-bound states in $Mb^{II}NO$ rebind at the same temperature, it also demonstrates that the rebinding rates of NO to the two ligand-bound states of ferrous myoglobin are approximately equal. This result is in contrast to the ligand-bound states of horse MbCO, where the higher frequency state (1945 cm^{-1}) reappears faster than the lower frequency state (1945 cm^{-1}) (Ansari et al., 1987; Chance et al., 1987; Mourant et al., 1993).

The ligand-bound states of $Mb^{III}NO$ and $Mb^{III}(H64L)NO$ can be seen in Figure 4. For both the native and mutant sample, single ligand-bound states are observed. For wild-type $Mb^{III}NO$, ν(N−O) falls at 1927 cm^{-1}. This band shifts to 1904 cm^{-1} for the mutant. The relative rebinding rates of NO to both the ferrous and ferric ligand-bound states are similar to each other, i.e., NO completely rebound in both cases by 30 K.

Photoproduct States of MbNO

Two photoproduct states are observed for $Mb^{II}NO$. For $Mb^{14}NO$, these modes appear at 1852 and 1857 cm^{-1} (Figure 5a). The photoproduct states shift to 1818 and 1824 cm^{-1} for $Mb^{15}NO$ (Figure 5b). The isotopic shifts are the same as those predicted by reduced mass calculation for $^{14}NO \rightarrow {}^{15}NO$, which are $\sim$33 cm^{-1}. Unlike the ligand-bound states, the rebinding rates from the two photoproduct states are significantly different from each other, where the 1852 cm^{-1} mode rebinds faster (i.e., at a lower temperature) than the 1857 cm^{-1} mode. Thus, there does not appear to be a direct correlation between the disappearance of each individual photoproduct state and the appearance of a corresponding ligand-bound state, suggesting interconversion of the photoproduct states before rebinding, analogous to MbCO

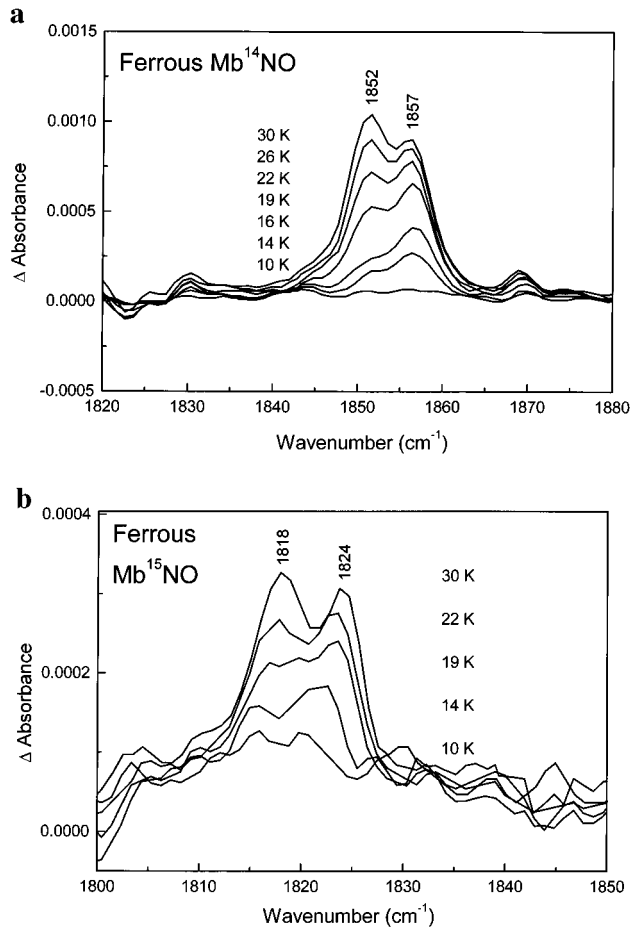

FIGURE 5: FTIR (photolyzed/unphotolyzed) difference spectra of (a) ferrous $Mb^{14}NO$ and (b) ferrous $Mb^{15}NO$, demonstrating the photoproduct conformational substates of $Mb^{II}NO$. Sample details, the photolysis protocol, and the method for generating difference spectra are described in Figure 3.

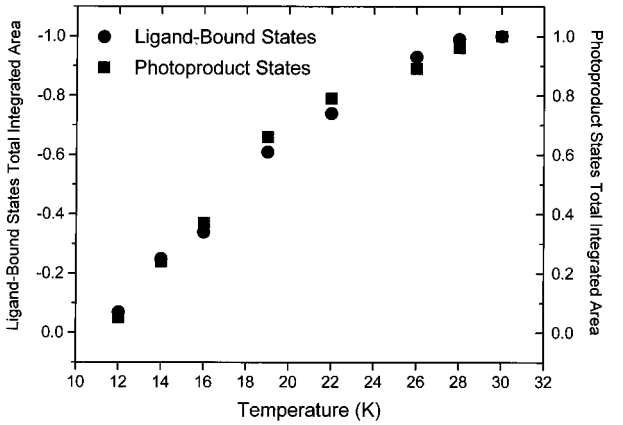

FIGURE 6: Fraction of the total integrated area for the ligand-bound states (data from Figure 3a) and the photoproduct states (data from Figure 5a) of $Mb^{II}NO$, as a function of temperature. Difference spectra were generated by dividing the photolyzed $Mb^{II}NO$ spectrum at 7 K by the partially-rebound spectra at each indicated temperature. Thus, the largest differences (and greatest area, i.e., −1.0 or 1.0 for the ligand-bound and photoproduct states, respectively) occur at 30 K. This figure demonstrates a stoichiometric relationship between the appearance of the ligand-bound states versus the disappearance of the photoproduct states as a function of rebinding temperature.

(Mourant et al., 1993). However, Figure 6 demonstrates a stoichiometric relationship between the *total* integrated area under the ligand-bound state bands versus the *total* integrated area under the photoproduct state bands as a function of temperature.

DISCUSSION

Ferrous Nitrosyl Myoglobin ($Mb^{II}NO$)

Ligand-Bound Conformational Substates

The NO molecule is well-characterized by infrared spectroscopy in both the free gas and metal-bound states (Cotton & Wilkinson, 1980). It has an unpaired electron in a π^* orbital, partially canceling out the effect of the π-bonding electrons, yielding a bond order of 2.5. In the free gas state, ν(N−O) is 1840 cm^{-1}. When the unpaired π^* electron is lost in NO^+ the bond becomes stronger, increasing ν(N−O) to 2150−2400 cm^{-1}, depending on its environment.

Unlike CO and O_2, NO is capable of binding to both ferrous and ferric hemes. The vibrational stretching frequency, ν(N−O), is very sensitive to the oxidation state of the iron and, hence, the structure of the Fe−N−O complex. When NO binds to a ferric heme, the unpaired π^* electron is able to backbond into the iron 3d orbitals, increasing the NO bond order to >2.5. Conversely, when NO binds to a ferrous heme, the unpaired π^* electron remains localized on NO, as opposed to backbonding into the already-reduced ferrous iron. This also causes the NO ligand to bend with respect to the heme plane, similar to MbO_2 (Wayland et al., 1974) and reducing the NO bond order to <2.5. Therefore, ν(N−O) is significantly lower for $Mb^{II}NO$ versus $Mb^{III}NO$ (*vida infra*).

A single ν(N−O) stretch has been assigned for $Mb^{II}NO$ using resonance Raman (1623 cm^{-1}; Benko & Yu, 1983; Tsubaki & Yu, 1982) and infrared (1612 cm^{-1}; Zhao et al., 1994) spectroscopies. In this study, we observe two bands (1607 and 1613 cm^{-1}) corresponding to conformational substates of horse $Mb^{II}NO$, where the primary ν(N−O) falls at 1613 cm^{-1}, in agreement with the earlier infrared studies. For horse skeletal muscle MbCO, infrared studies have also identified two ligand-bound conformational substates, which are easily resolved because they are separated by ∼20 cm^{-1} and fall into an infrared region void of protein absorption (Miller, 1995). Since the $Mb^{II}NO$ substates are separated by only 5−6 cm^{-1}, earlier work using $^{14}NO/^{15}NO$ difference spectroscopy was most likely not sensitive enough to resolve these substates.

For wild-type MbCO, the ligand-bound substate at 1945 cm^{-1} is thought to have a polar interaction between the CO ligand and the distal histidine. This polar interaction is absent when the distal histidine is replaced by leucine, and a single conformational substate exists at 1966 cm^{-1}. Conformational substates have also been suggested for MbO_2, where differences in hydrogen bonding between the O_2 ligand and the distal histidine give rise to two different modes (Miller & Chance, 1995; Miller et al., 1996; Potter et al., 1987). A hydrogen bond between the NO ligand and the distal histidine has been proposed based on ENDOR (Kappl & Hutterman, 1989) and other EPR investigations (Ikeda-Saito et al., 1991), although the bond may be weak (Lee et al., 1994). For $Mb^{II}NO$, we suspect that both modes (1607 and 1613 cm^{-1}) are due to conformations involving an interaction between the NO ligand and the distal histidine, since the two substates are only separated by 6 cm^{-1}.

Photoproduct Conformational Substates

As can be seen from Figure 3, the ligand-bound states in $Mb^{II}NO$ appear at approximately equal rates as the sample is warmed. However, Figure 5 demonstrates that the two photoproduct states (1852 and 1857 cm^{-1}) disappear at significantly different rates, implying that the specific ligand-bound states do not correspond to specific photoproduct states. But there is a stoichiometric relationship between the *total appearance* of the ligand-bound states versus the *total disappearance* of the photoproduct states as a function of rebinding temperature. This can be seen in Figure 6. The interconversion of the photoproduct states before rebinding has also been observed for MbCO (Mourant et al., 1993). Frauenfelder and co-workers showed that the barrier for interconversion between ligand-bound states is too high at cryogenic temperatures (<180 K), but the photoproduct states can interconvert even at 10 K.

A combination of the crystallographic structure of Mb*CO (Schlichting et al., 1994), the photoproduct infrared conformational states (Braunstein et al., 1993; Mourant et al., 1993), and the myriad of room temperature studies of NO binding to native and mutant myoglobins in the picosecond time regime helps provide a structural understanding of the roles of various distal pocket residues in the NO rebinding process (Carlson et al., 1994; Carver et al., 1990; Gibson et al., 1992; Ikeda-Saito et al., 1993; Olson & G. N. Phillips, 1996). Since NO reacts with the heme iron very rapidly, the distal pocket structure plays an important role in determining the ligand-rebinding barrier from the distal pocket. For example, the substitution of bulky side chains at positions 29 and/or 68 prevents the NO ligand from escaping from the iron coordination sphere, resulting in rapid recombination (Carlson et al., 1994). Likewise, replacing the distal histidine with small residues also contributes to faster NO recombination because it's thought that the distal histidine pushes the NO ligand away from the heme iron upon photolysis (Quillin et al., 1995).

The crystal structure of the MbCO photoproduct at 20 K indicates that the CO ligand resides in the center of the heme pocket, parallel to the heme plane (Schlichting et al., 1994). It is located 3.9 Å from the distal histidine, so any strong interaction between CO and the distal pocket residues is minimal. This is supported by the relative insensitivity of the photoproduct state frequency to distal pocket mutations and pH (Braunstein et al., 1993; Mourant et al., 1993). Since it is unclear whether the C or the O atom is closest to the heme iron, the different photoproduct states are thought to be due to different interactions of the CO ligand with the heme itself, which result from small rotation or translations of the free CO in the distal pocket (Lim et al., 1995).

The photoproduct states of $Mb^{II}NO$ (Figure 5) are strongly analogous to those of MbCO. First, we observe two photoproduct states, where the difference in frequency between the two states may be related to different interactions between the NO ligand and the heme π-electron system. Second, the photoproduct states are separated from each other by 5−6 cm^{-1}, and are reasonably close to the free gas values (MbCO, 2143 cm^{-1}; $Mb^{II}NO$, 1840 cm^{-1}) (Cotton & Wilkinson, 1980). Third, the photoproduct state with the lower frequency (1852 cm^{-1}) rebinds faster than the higher frequency photoproduct state (1857 cm^{-1}). Thus similar to MbCO (Lim et al., 1995), we suggest that the two photoproduct states of $Mb^{II}NO$ are roto-isomers, where the fast-rebinding state has the N atom oriented closer to the iron. The slow-rebinding isomer has the O atom closer to the iron, so that the NO must "flip" before rebinding.

Since the ligand-bound states are only separated by 6 cm^{-1}, we propose that *both* ligand-bound modes in $Mb^{II}NO$ are due to configurations involving an interaction between the NO ligand and the distal histidine, unlike MbCO. Upon photolysis, the distal histidine "pushes" the NO ligand into the distal pocket. The "free" NO molecule is capable of small rotations in the distal pocket, depending upon the specific ligand trajectory. It is possible that the "slow" rebinding photoproduct state (1857 cm^{-1}) arises from a ligand trajectory which allows the NO to flip in the distal pocket, so that it must flip back before rebinding. Conversely, the trajectory for the "fast" rebinding photoproduct state (1852 cm^{-1}) does not permit this rotation.

Ferric Nitrosyl Myoglobin ($Mb^{III}NO$)

Ligand-Bound Conformational Substates

$Mb^{III}NO$ is isoelectronic with MbCO, suggesting a linear Fe−N−O moiety. However, resonance Raman has been used to show that ν(Fe−NO) for $Mb^{III}NO$ is 595 cm^{-1}, ∼90 cm^{-1} higher than ν(Fe−CO) for MbCO (Benko & Yu, 1983). The unusually strong Fe−NO bond is attributed to back-bonding from the unpaired electron in the π^*(NO) orbital. Consequently, this backbonding is expected to decrease ν-(N−O), as compared to ν(C−O). This is consistent with what Caughey and co-workers observed for $Hb^{III}NO$ (Sampath et al., 1994) and with the data we present here: we find ν(N−O) for $Mb^{III}NO$ at 1927 cm^{-1}, whereas ν(C−O) for $Mb^{II}CO$ falls between 1940 and 1965 cm^{-1} (Ansari et al., 1987; Austin et al., 1975; Chance et al., 1987).

Structurally, the Fe−C−O linkage in MbCO is linear and the conformational substates in MbCO have been attributed to different distal pocket interactions with the linearly-bound CO ligand, which influence the degree of $Fe_{d\pi} \rightarrow CO_{\pi^*}$ backbonding (Hu et al., 1994; Li et al., 1994; Li & Spiro, 1988; Ray et al., 1994). Since $Mb^{III}NO$ and $Mb^{II}CO$ are isoelectronic, it is expected that similar interactions would exist between the NO ligand and the distal residues. For wild-type $Mb^{III}NO$, a single conformational substate with respect to ν(N−O) is observed at 1927 cm^{-1}. When the distal histidine is replaced by leucine, the ferric ligand-bound state shifts to *lower* frequency (1904 cm^{-1}), contrary to ν-(C−O) in the Mb(H64L)CO mutant. So why does an NO-distal histidine interaction cause a 20 cm^{-1} shift to *higher* frequency whereas a CO-distal histidine interaction results in a similar shift to *lower* frequency?

It is likely that the NO ligand is involved in a negative ($\delta-$) polar interaction with the distal histidine (Figure 7). When NO binds to a ferric iron, a resonance structure favoring a positive NO ligand and a ferrous iron exists: $Fe^{(\delta-)}—N{\equiv}O^{(\delta+)}$. Tautomerism of the distal histidine occurs, such that the N_ϵ is unprotonated and able to accept positive charge from the NO ligand. Thus, the bond order of NO would increase, increasing ν(N−O) as compared to Mb^{III}-(H64L)NO, where the distal hisitidine is absent (Li et al., 1994; Li & Spiro, 1988; Ray et al., 1994). A similar interaction has been suggested between aquomet myoglobin, $Mb^{III}OH_2$, and the distal histidine (La Mar et al., 1988).

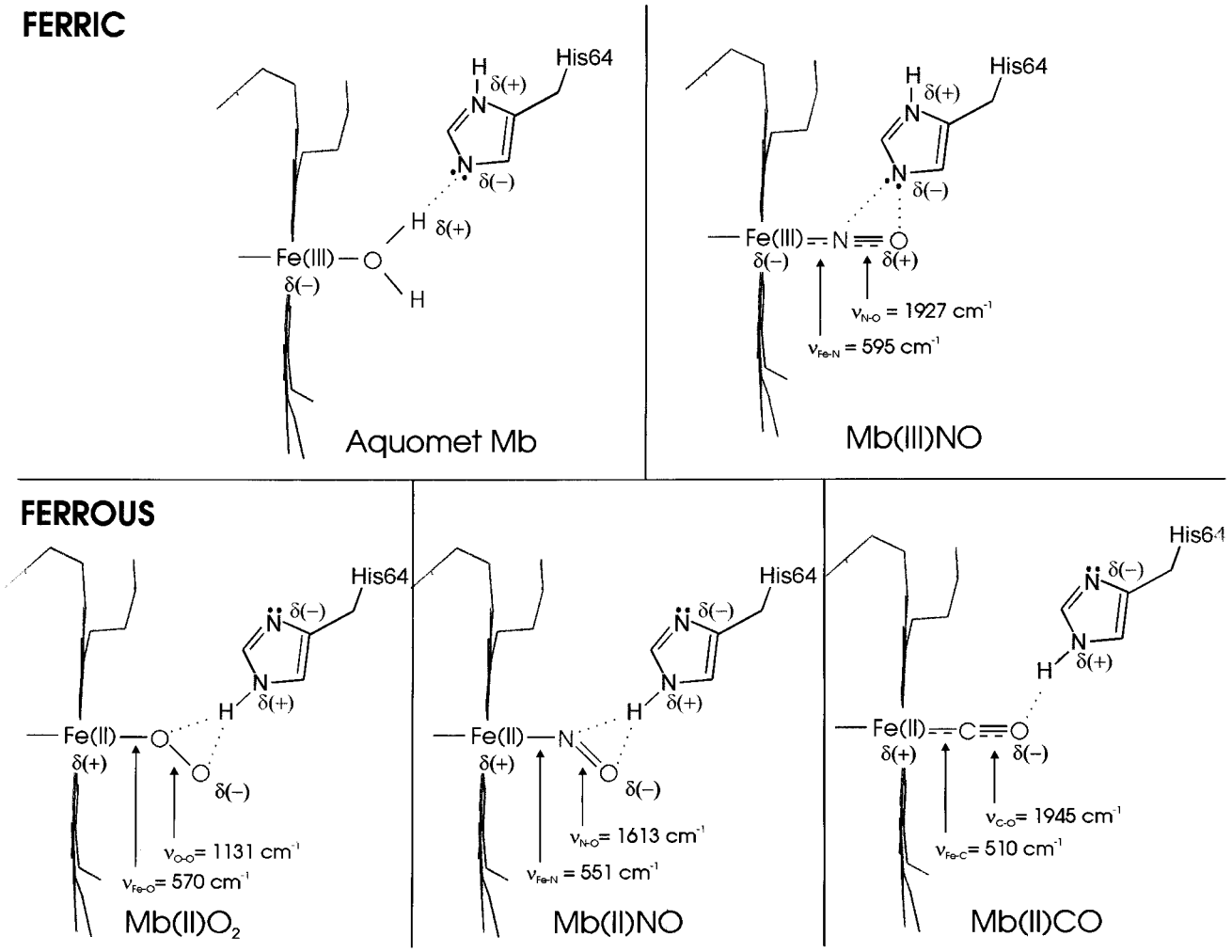

FIGURE 7: Demonstration of the different polar interactions that occur between the distal histidine of ferric and ferrous myoglobin and NO, CO, O_2, and H_2O. Tautomerism of the distal histidine results in positive ($\delta+$) polar interactions between N_ϵ and the ligand (NO, CO, and O_2) in ferrous hemes and negative ($\delta-$) polar interactions between N_ϵ and the ligand (NO and H_2O) in ferric hemes.

Conformational substates involving tautomers of the distal hisitidine in MbCO have already been suggested by several groups (Jewsbury & Kitagawa, 1994, 1995, Oldfield et al., 1991). When CO binds to myoglobin, a $Fe^{(\delta+)}$—$C{\equiv}O^{(\delta-)}$ moiety exists, favoring the distal histidine tautomer in which the N_ϵ of the distal histidine is protonated. In this case, a positive ($\delta+$) polar interaction with the distal histidine occurs, where N_ϵ donates a proton to the CO ligand, reducing its bond order and decreasing ν(C−O).

Photoproduct Conformational Substates

Photolysis of NO from ferric myoglobin results in a five-coordinate, ferric heme (Kobayashi et al., 1980). Mutant myoglobins with apolar residues substituted for the distal histidine are also five-coordinate in the ferric form (Morikis et al., 1990; Quillin et al., 1993), making them good models for ferric Mb*NO. The Soret band in these mutants falls near ~393 nm, consistent with our results. The photoproduct yield for $Mb^{III}NO$ is significantly less than Mb^{III}(H64L)NO (Figure 2), suggesting a lower barrier to rebinding for native $Mb^{III}NO$. Since NO is extremely reactive with the iron atom, the orientation of the ligand in distal pocket "docking sites" primarily determine the ligand rebinding barrier (Gibson et al., 1992; Jongeward et al., 1988; Olson & G. N. Phillips, 1996). Picosecond kinetic data have shown than the free volume of the distal pocket greatly affects the NO recombination barrier. Bulky side chains at positions 29 and/or 68 prevent the NO ligand from escaping from the iron coordination sphere, resulting in rapid recombination (Carlson et al., 1994). Likewise, it is thought that the distal histidine pushes the NO ligand away from the heme iron upon photolysis, so that replacing it with small residues also contributes to faster NO recombination (Quillin et al., 1995).

In wild-type ferric myoglobin, there is a water molecule in the sixth coordination position, which must be displaced for NO to bind. Room temperature rebinding measurements have shown that the rate determining step is the displacement of the water bound to the ferric iron (Olson & G. N. Phillips, 1996). It is unclear whether this water molecule remains in the distal pocket after the ligand binds (as it does in MbO_2, but not in MbCO), since crystallographic data are not available for $Mb^{III}NO$. If so, it will decrease the free volume available to the NO ligand after photolysis, preventing the NO ligand from leaving the vicinity of the heme iron, resulting in a low recombination barrier and a low photoproduct yield. In contrast to wild-type ferric myoglobin, resonance Raman (Morikis et al., 1990) and X-ray crystallographic (Quillin et al., 1993) data indicate that ferric myoglobin mutants which have the distal histidine replaced by an apolar residue exclude water from the distal pocket, resulting in a five-coordinate species. For the mutant, Mb^{III}-(H64L)NO, absence of water in the distal pocket may

increase the free volume available to the photolyzed ligand, allowing it to travel further from the heme iron, increasing the barrier to rebinding and the photoproduct yield.

The photolyzed/unphotolyzed FTIR difference spectra of ferric MbNO failed to show any infrared modes for the photoproduct states within the signal/noise ratio of our spectra ($<10^{-4}$ OD from 1500−2500 cm^{-1}). This result suggests that the photoproduct yields for the ferric species are not high enough to produce observable photoproduct states. In the data we present here, the intensity of the ligand bound state for Mb^{III}(H64L)NO is ∼0.0015 OD. Since the oscillator strength of the photoproduct state is only ∼5% of the ligand-bound state, the expected intensity of the photoproduct state is at the limit of the signal/noise ratio for our experiments. Additional experiments with Mb^{III}NO mutants with higher photoproduct yields will be necessary to further probe the infrared spectra of the cryogenic Mb^{III}NO photoproduct states.

SUMMARY AND OUTLOOK

We have demonstrated that photolyzed/unphotolyzed FTIR spectroscopy is a promising method for investigating the numerous ways in which NO reacts with hemeproteins. For myoglobin, this technique was used to show that NO binds to a ferrous heme in two different conformations, each having similar rebinding rates. Photolysis of NO results in two conformational substates which have significantly different binding rates which may be ascribed to roto-isomers of the free NO in the heme pocket. Significant changes occur in the bonding structure of ferric MbNO, as evidenced by a ∼300 cm^{-1} increase in ν(N−O). In addition, replacement of the distal histidine with a leucine residue in ferric MbNO causes a 20 cm^{-1} *decrease* in ν(N−O), contrary to the analogous MbCO mutant. These results suggest tautomerism of the distal histidine such that a negative ($\delta-$) polar interaction occurs between the NO ligand and an unprotonated N_ϵ and a positive ($\delta+$) polar interaction occurs between a protonated N_ϵ and the CO ligand.

In the future, we hope to extend this technique to additional myoglobin mutants and also other nitrosyl hemeprotein systems such as nitric oxide synthase, cytochrome *c* oxidase, hemoglobin, and guanylate cyclase. For myoglobin mutants, altering the architecture of the heme pocket should provide a method for "tuning" the cryogenic photoproduct yield. For example, mutations at His-64, Leu-29, and/or Val-68 affect steric restrictions on the ligand and its access to the heme iron, which clearly influences the rebinding barrier (Olson & G. N. Phillips, 1996). Higher photoproduct yields will allow the observance of the photoproduct states in Mb^{III}NO, so that the electronic interactions of the photolyzed NO can be compared to those of its ferrous counterpart. For Mb^{II}NO, the presence of a hydrogen bond between NO and the distal histidine is directly testable by examining the ligand-bound states of Mb^{II}(H64L)NO. Analogous to MbCO, ν(N−O) is expected to increase in the absence of the distal side interaction. The photoproduct states of this mutant will also probe the sensitivity of the free NO ligand to a different ligand trajectory and/or "docking sites" caused by the absence of the distal histidine. Overall, a comparison of the ligand-bound states, photoproduct states, and rebinding rates will be useful in developing an understanding of how different NO-binding mechanisms dictate the nitrosyl hemeprotein function.

ACKNOWLEDGMENT

The authors thank the reviewers for a critical evaluation of this manuscript, valuable input toward data interpretation, and for suggesting Figure 7.

REFERENCES

Ansari, A., Berendzen, J., Braunstein, D., Cowen, B. R., Fraunfelder, H., Hong, M. K., Iben, I. E. T., Johnson, J. B., Ormos, P., Sauke, T. B., Scholl, R., Schulte, A., Steinbach, P. J., Vittitow, J., & Young, R. D. (1987) *Biophys. Chem. 26*, 337.

Austin, R. H., Beeson, K., Eisenstein, L., Frauenfelder, H., & Gunsalus, I. C. (1975) *Biochemistry 14*, 5355−5373.

Benko, B., & Yu, N. T. (1983) *Proc. Natl. Acad. Sci. U.S.A. 80*, 7042−7046.

Berendzen, J., & Braunstein, D. (1990) *Proc. Natl. Acad. Sci. U.S.A. 87*, 1−5.

Braunstein, D. P., Chu, K., Egeberg, K. D., Frauenfelder, H., Mourant, J. R., Nienhaus, G. U., Ormos, P., Sligar, S. G., Springer, B. A., & Young, R. D. (1993) *Biophys. J. 65*, 2447−2454.

Brudwig, G. W., Stevens, T. H., & Chan, S. I. (1980) *Biochemistry 19*, 5275−5285.

Carlson, M. L., Regan, R., Elber, R., Li, H., Phillips, G. N., Olson, J. S., & Gibson, Q. H. (1994) *Biochemistry 33*, 10597−10606.

Carver, T. E., Rohlfs, R. J., Olson, J. S., Gibson, Q. H., Blackmore, R. S., Springer, B. A., & Sligar, S. G. (1990) *J. Biol. Chem. 265*, 20007−20020.

Chance, M. R. (1993) *Methods Enzymol. 226*, 97−118.

Chance, M. R., Campbell, B. F., Hoover, R., & Friedman, J. M. (1987) *J. Biol. Chem. 262*, 6959−6961.

Cotton, F. A., & Wilkinson, G. (1980) *Advanced Inorganic Chemistry*, 4th ed., John Wiley and Sons, New York.

Gibson, Q. H., Regan, R., Elbers, R., Olson, J. S., & Carver, T. E. (1992) *J. Biol. Chem. 267*, 22022−22034.

Hu, S., Vogel, K. M., & Spiro, T. G. (1994) *J. Am. Chem. Soc. 116*, 11187−11188.

Ignarro, L. J., Fukuto, J. M., Griscavage, J. M., Rogers, N. E., & Byrnes, R. E. (1993) *Proc. Natl. Acad. Sci. U.S.A. 90*, 8103−8107.

Ikeda-Saito, M., Dou, Y., Yonetani, T., Olson, J. S., Li, T., Regan, R., & Gibson, Q. H. (1993) *J. Biol. Chem. 268*, 6855−6857.

Ikeda-Saito, M., Lutz, R. S., Shelley, D. A., McKelvey, E. J., Mattera, R., & Hori, H. (1991) *J. Biol. Chem. 266*, 23641−23647.

Jewsbury, P., & Kitagawa, T. (1994) *Biophys. J. 67*, 2236−2250.

Jewsbury, P., & Kitagawa, T. (1995) *Biophys. J. 68*, 1283−1294.

Jia, L., Bonaventura, C., Bonaventura, J., & Stamler, J. S. (1996) *Nature 380*, 221−226.

Jongeward, K. A., Magde, D., Taube, D. J., Marsters, J. C., Traylor, T. G., & Sharma, V. S. (1988) *J. Amer. Chem. Soc. 110*, 380−387.

Kappl, R., & Hutterman, J. (1989) in *Advanced EPR Applications in Biology and Biochemistry* (Hoff, A. J., Ed.), Elsevier Science Publishing Company, Inc., Amsterdam.

Kobayashi, K., Tamura, M., Hayashi, K., Hori, H., & Morimoto, H. (1980) *J. Biol. Chem. 255*, 2239−2242.

La Mar, G. N., Chatfield, M. J., Peyton, D. H., de Ropp, J. S., Smith, W. S., Drishnamoorthi, R., Satterlee, J. D., & Erman, J. E. (1988) *Biochim. Biophys. Acta 956*, 267−276.

Lee, H. C., Peisach, J., Dou, Y., & Ikeda-Saito, M. (1994) *Biochemistry 33*, 7609−7618.

Li, T., Quillin, M. L., Phillips, G. N., & Olson, J. S. (1994) *Biochemistry 33*, 1433−1446.

Li, X. Y., & Spiro, T. G. (1988) *J. Am. Chem. Soc. 110*, 6024−6033.

Lim, M., Jackson, T. A., & Anfinrud, P. A. (1995) *Science 269*, 962−966.

Matsuoka, A., Stuehr, D. J., Olson, J. S., Clark, P., & Ikeda-Saito, M. (1994) *J. Biol. Chem. 269*, 20335−20339.

Miller, L. M. (1995) Ph.D. Thesis, Department of Physiology and Biophysics, Albert Einstein College of Medicine, New York, NY.
Miller, L. M., & Chance, M. R. (1994) *J. Am. Chem. Soc. 116*, 9662−9669.
Miller, L. M., & Chance, M. R. (1995) *Biochemistry 34*, 10170−10179.
Miller, L. M., Patel, M., & Chance, M. R. (1996) *J. Am. Chem. Soc. 118*, 4511−4517.
Moncada, S., & Higgs, A. (1993) *N. E. J. Med. 329*, 2002−2012.
Morikis, D., Champion, P. M., Springer, B. A., & Sligar, S. G. (1989) *Biochemistry 28*, 4791−4800.
Morikis, D., Champion, P. M., Springer, B. A., Egeberg, K. D., & Sligar, S. G. (1990) *J. Biol. Chem. 265*, 12143−12145.
Mourant, J. R., Braunstein, D. P., Chu, K., Frauenfelder, H., Nienhaus, G. U., Ormos, P., & Young, R. D. (1993) *Biophys. J. 65*, 1496−1507.
Nathan, C. (1992) *FASEB J. 6*, 3051−3064.
Oldfield, E., Guo, K., Augspurger, J. D., & Dykstra, C. E. (1991) *J. Am. Chem. Soc. 113*, 7537−7541.
Olson, J. S., & G. N. Phillips, J. (1996) *J. Biol. Chem. 271*, 17593−17596.
Phillips, S. E. V. (1980) *J. Mol. Biol. 142*, 531−554.
Phillips, S. E. V., & Schoenborn, B. P. (1981) *Nature 292*, 81−82.
Potter, W. T., Tucker, M. P., Houtchens, R. A., & Caughey, W. S. (1987) *Biochemistry 26*, 4699−4707.
Quillin, M. L., Arduini, R. M., Olson, J. S., & Phillips, G. N. (1993) *J. Mol. Biol. 234*, 140−155.
Quillin, M. L., Li, T., Olson, J. S., Phillips, G. N., Dou, Y., Ikeda-Saito, M., Regan, R., Carlson, M., Gibson, Q. H., Li, H., & Elber, R. (1995) *J. Mol. Biol. 245*, 416−436.
Ray, G. B., Li, X. Y., Ibers, J. A., Sessler, J. L., & Spiro, T. G. (1994) *J. Am. Chem. Soc. 116*, 162−176.
Sampath, V., Zhao, X. J., & Caughey, W. S. (1994) *Biochem. Biophys. Res. Commun. 198*, 281−7.
Schlichting, I., Berendsen, J., Phillips, G. N., & Sweet, R. M. (1994) *Nature 371*, 808−812.
Springer, B. A., & Sligar, S. G. (1987) *Proc. Natl. Acad. Sci. U.S.A. 84*, 8961−8965.
Stamler, J. S., Singel, D. S., & Loscalzo, J. (1992) *Science 258*, 1898−1902.
Stone, J. R., & Marletta, M. A. (1994) *Biochemistry 33*, 5636−5640.
Stuehr, D. J., & Ikeda-Saito, M. (1992) *J. Biol. Chem. 267*, 20547−20550.
Tsubaki, M., & Yu, N. T. (1982) *Biochemistry 21*, 1140−1144.
Wayland, B. B., Minkiewicz, J. V., & Abd-Elmageed, M. E. (1974) *J. Am. Chem. Soc. 96*, 2795−2801.
Zhao, X. J., Sampath, V., & Caughey, W. S. (1994) *Biochem. Biophys. Res. Commun. 204*, 537−543.

BI962744O